

Radial profiles of ground-state transitions of heliumlike argon from the Alcator-C tokamak

J. E. Rice and E. S. Marmor

Plasma Fusion Center, Massachusetts Institute of Technology, Cambridge, Massachusetts 02139

E. Källne and J. Källne

Joint European Tokamak, Culham Laboratory, EURATOM—United Kingdom Atomic Energy Authority Fusion Association, Abingdon-on-Thames, OX14 3EA Oxfordshire, United Kingdom

(Received 11 August 1986)

Spectra of the complete series of ground-state transitions in heliumlike Ar^{16+} ($1snp-1s^2$, for $2 \leq n < 50$) have been obtained from the Alcator-C tokamak with use of a compact x-ray crystal spectrometer. Radial profiles of these transitions have been measured and have been compared with the results of a transport model which includes the basic atomic processes. In the plasma center, collisional excitation is the most important population mechanism for the upper levels. For the outer regions of the plasma ($r/a_L > 0.5$), recombination of Ar^{17+} is the dominant population process for upper levels of most transitions, and preferentially populates the $n=2$ triplet levels. Impurity transport provides sufficient amounts of hydrogenlike argon at the cooler, outer radii. For the high- n transitions $1s9p-1s^2$ and $1s10p-1s^2$, charge-exchange recombination is the dominant population mechanism at the plasma edge under certain operating conditions. The intensities of these lines have been used to determine neutral-hydrogen density profiles. For ground-state transitions with $n > 13$, charge transfer from excited neutral hydrogen is the only important population process for $r/a_L > 0.5$.

I. INTRODUCTION

Recently, there has been considerable interest in x-ray spectroscopy of highly ionized atoms in high-temperature tokamak plasmas.^{1–20} Of particular interest are $\Delta n = 1$ x-ray spectra from heliumlike species of medium- Z impurities.^{4,5,7–9,11–17,20} Most measurements on tokamaks have been obtained using large spectrometers with Rowland circle geometry, which because of size constraints, are restricted to view along central chords. In the center of high-temperature plasmas, electron-impact excitation is the most important mechanism for populating the upper levels of the observed transitions. For the measurements described in this paper, x-ray spectra of heliumlike $^{18}\text{Ar}^{16+}$ have been obtained with a compact spectrometer of Von Hamos geometry, which has been scanned radially to obtain spectra from all regions of the plasma, including the edge. In the regions of the plasma where the electron temperature is much lower than the transition energy of the observed lines, radiative recombination of $^{18}\text{Ar}^{17+}$ is the most important process for populating most of the upper levels in $^{18}\text{Ar}^{16+}$. The key to the existence of this condition is that the outward radial transport time of $^{18}\text{Ar}^{17+}$ from the hot plasma core is comparable to the recombination times, so that hydrogenlike argon exists in the very cool regions near the edge. Also near the plasma edge, where the neutral-hydrogen density is relatively high, charge-transfer recombination is found to be very important in populating certain levels in $^{18}\text{Ar}^{16+}$ both by direct recombination and through subsequent cascades.

The spectrometer system and experimental conditions are described in Sec. II. Ground-state transitions of heliumlike argon from the $n=2$ level, in addition to several

satellite lines, have been identified and are presented in Sec. III. Radial brightness profiles of the $^{18}\text{Ar}^{16+}$ emission features have been measured and are shown in Sec. IV. Section V is devoted to the modeling of the radial brightness profiles of the four main lines in the heliumlike spectrum. Radial profiles of ground-state transitions from high- n levels ($3 < n < 13$) in heliumlike argon and observations of charge-exchange recombination are shown in Sec. VI. Determination of the neutral-hydrogen density profile is described in Sec. VII. In Sec. VIII are presented observations of very-high- n ($15 < n < \infty$) transitions to the ground state in $^{18}\text{Ar}^{16+}$. Radial profiles of satellite transitions are shown in Sec. IX.

II. SPECTROMETER SYSTEM AND EXPERIMENTAL CONDITIONS

X-ray spectra from highly ionized argon^{8,9,14,16–19} have been obtained from the Alcator-C (Ref. 21) tokamak using a compact x-ray crystal spectrometer. The spectrometer system has been described in detail elsewhere^{16,17,22} and some relevant features are summarized here. The Von Hamos-type instrument was employed with a 2.5 cm \times 2.5 cm quartz crystal ($2d = 6.687 \text{ \AA}$) and a radius of curvature of 50 cm. The x rays were dispersed onto a five wire, position-sensitive delay line proportional counter with an active area of 3.5 cm \times 1.0 cm, which utilized a krypton-ethane gas flow. The wavelength range from 2900 to 4100 mÅ was available for the configuration used in these experiments, with a 100-mÅ increment for each spectrometer setting. Large composite spectra were then obtained by adding several overlapping spectra. Individual line shapes were dominated by Doppler broaden-

ing as the resolving power of the spectrometer was 2500. Due to the compact size of the instrument, radial (vertical) scans could be performed by tilting in a plane perpendicular to the toroidal magnetic field. The spatial resolution of 3 cm was determined largely by the slit height. The spectrometer was able to be scanned in chord height d from the plasma center ($d=0$) to outside the limiter radius ($d > a_L$).

Measurements described in this paper were from plasmas with limiter radii a_L of 12.5 and 16.5 cm. The toroidal magnetic field was in the range from 80 to 100 kG, hydrogen, deuterium, and helium working gases were used, and the average electron density was in the range $(1.0-2.5) \times 10^{14} \text{ cm}^{-3}$. Density profiles were taken to have the form $n_e = n_{e0} [1 - (r/a_L)^2]^\alpha$ with α in the range from 0.5 to 1.0. Electron temperature profiles were of the form $T_e = T_{e0} \exp[-(r/a_T)^2]$, where a_T generally depends on plasma parameters as $a_T^2 = \frac{3}{2} (q_0/q_L) a_L^2$ with q_0 and q_L the central and limiter safety factors.

Argon was introduced into the torus through a fast piezoelectric valve. The argon subsequently recycled and reached a steady-state level in the plasma for typically a 200 ms duration, during which time the measurements were made. Concentrations were in the range from 10^{-5} to 10^{-3} of the electron density.

III. $\Delta n = 1$ SPECTRA OF He-LIKE ARGON

In Fig. 1 is plotted a spectrum of $^{18}\text{Ar}^{16+}$ taken from five similar discharges with $\bar{n}_e = 2.4 \times 10^{14} \text{ cm}^{-3}$, $T_{e0} = 1650 \text{ eV}$, $B_T = 80 \text{ kG}$, and $I = 275 \text{ kA}$. The strongest lines are the resonance (w, 3.949 Å), forbidden (z, 3.994 Å), and intercombination lines (x, 3.966 Å and y, 3.969 Å) (Refs. 7, 8, 20, and 22), and several satellite transitions from lithiumlike (with the spectator electron in the

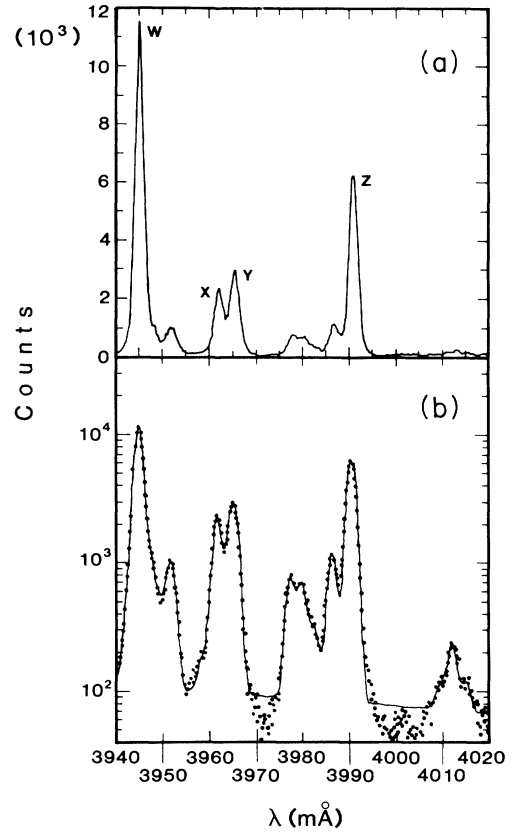


FIG. 1. Spectrum of $\Delta n = 1$ ground-state transitions of heliumlike argon in the wavelength region from 3.94 to 4.02 Å (a) on a linear scale and (b) on a logarithmic scale including fit.

TABLE I. Measured and theoretical wavelengths and configurations for $\Delta n = 1$ transitions.

Name	Transition	Rel. int.	λ	λ_{VS}^{23}	λ_{BT}^{24}	λ_{TFR}^{14}	λ_{VS}^{25}
w	$1s2p3d^2P_{3/2} - 1s^23d^2D_{5/2}?$	0.026	3.9464	3.9449			
	$1s2p^1P_1 - 1s^2^1S_0$	1.000	3.9492	3.9482		3.9451	3.9492
	$1s2p3d^2F_{7/2} - 1s^23d^2D_{5/2}?$	0.087	3.9520	3.9498		3.9458	
3	$1s2p3p^2D_{5/2} - 1s^23p^2P_{1/2}?$	0.032	3.9547	3.9543			
	$1s2p3p^2D_{5/2} - 1s^23p^2P_{3/2}$	0.072	3.9563	3.9553			
	$1s2p^2^2S_{1/2} - 1s^22p^2P_{1/2}?$	0.009	3.9625	3.9611			
x	$1s2p^3P_2 - 1s^2^1S_0$	0.207	3.9659	3.9649		3.9622	3.9660
y	$1s2p^3P_1 - 1s^2^1S_0$	0.269	3.9692	3.9683		3.9659	3.9694
q	$1s2s2p^2P_{3/2} - 1s^22s^2S_{1/2}$	0.059	3.9815	3.9806	3.9785	3.9777	
	$1s2p^2^2P_{3/2} - 1s^22p^2P_{1/2}$			3.9811			
r	$1s2s2p^2P_{1/2} - 1s^22s^2S_{1/2}$	0.051	3.9839	3.9827	3.9807	3.9801	
a	$1s2p^2^2P_{3/2} - 1s^22p^2P_{3/2}$	0.018	3.9864	3.9852	3.9826	3.9823	
k	$1s2p^2^2D_{3/2} - 1s^22p^2P_{1/2}$	0.096	3.9903	3.9892	3.9865	3.9866	
j	$1s2p^2^2D_{5/2} - 1s^22p^2P_{3/2}$			3.9932	3.9898	3.9907	
z	$1s2s^3S_1 - 1s^2^1S_0$	0.561	3.9943	3.9934		3.9909	3.9943

$n = 2, 3,$ and 4 levels) and berylliumlike argon are also seen. In the lower portion of the figure is a logarithmic plot of the data in addition to the fitted spectrum. The line shapes are assumed to be Gaussian and the fitting routine determines the amplitude, width, and position of a specified number of lines in the spectrum. The ion temperatures and hence the linewidths are taken to be the same for all the lines. Measured and theoretical^{14,23-25} wavelengths and configurations for the transitions studied here are given in Table I. No direct wavelength calibration has been made for these spectra so the quoted values are normalized to the theoretical values²⁵ for the resonance and forbidden lines, and the dispersion is assumed to be linear in the wavelength region in between.

IV. RADIAL PROFILES OF $\Delta n = 1$ TRANSITIONS IN He-LIKE ARGON

Radial brightness profiles have been obtained by vertically scanning the spectrometer on a shot to shot basis. Shown in Fig. 2 are spectra taken at several radial locations for a series of identical 80 kG, deuterium discharges with $a_L = 12.5$ cm. The top spectrum was obtained from the central chord where the central electron temperature was 1650 eV, and is indicative of normal operating conditions. In the second spectrum, taken at a chord height of 8 cm, the forbidden line is stronger than the resonance line and the satellites have also grown relative to w. The electron temperature was down a factor of 3 at 8 cm. In

the third spectrum, at a chord of 10.5 cm, the forbidden line dominates, and the satellites have disappeared. At 10.5 cm the temperature was about 250 eV. Nearly all that remains in the bottom spectrum is the forbidden line. This was obtained near the limiter radius where the electron temperature was about 100 eV. The spatial resolution of the instrument is ~ 3 cm. The lines are narrower at the outer radii mainly due to a decrease in the ion temperature as evidenced by the increase in the valley between the intercombination lines for successive spectra. Absence of dielectric satellites such as m, s, and t at the outer radii may also contribute to this.¹²

Shown in Fig. 3 are radial brightness profiles for the major components of the heliumlike argon spectrum from the series of identical discharges from which the spectra of Fig. 2 were obtained. The profiles were determined from the integrated intensities of the fitted spectra. The resonance line has the narrowest radial profile, and crosses the forbidden line profile at 8.0 cm and the intercombination line profiles at 9.8 cm. The forbidden line has the broadest radial profile. The overlapping satellite j has been subtracted from z using a constant factor of 1.3 times the intensity of k.⁸ The intercombination line profiles steadily converge with increasing radius. These lines also have some satellite admixture which has been ignored in this analysis. Plasma parameters for this series of discharges were $T_{e0} = 1650$ eV, $a_T = 7.5$ cm, $a_L = 12.5$ cm, $n_{e0} = 3.5 \times 10^{14}$ cm⁻³, and $\alpha = 1.0$.

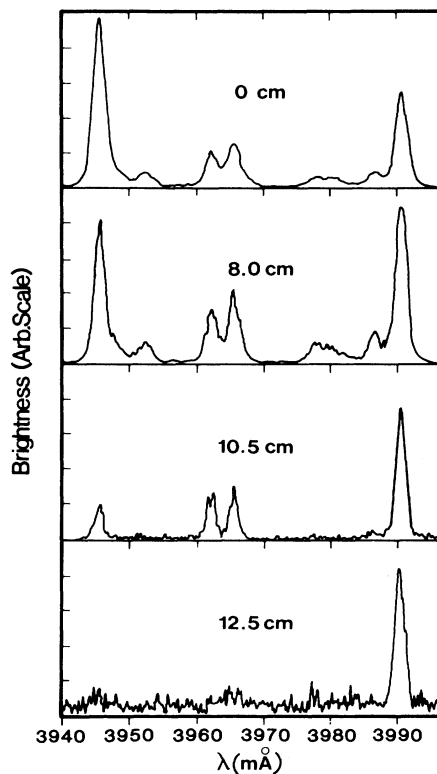


FIG. 2. Spectra of heliumlike argon at four different radial locations. Local electron temperatures for the four cases are 1650, 550, 250, and 100 eV. The vertical scales are all arbitrary.

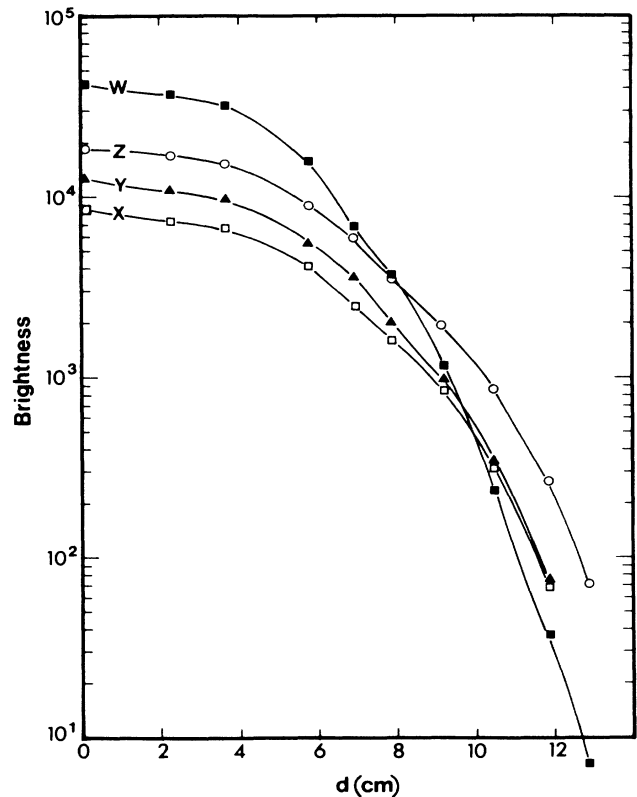


FIG. 3. Observed radial brightness profiles for different components of the heliumlike argon spectrum.

V. POPULATION MECHANISMS AND PREDICTED PROFILES

In an attempt to account for these observed brightness profiles, a model for heliumlike line intensities has been used.²⁶ Modeling of the relative intensities of lines from central chord measurements has previously been reported.^{12,14,15} Populations of the various levels are determined by a balance among radiative transitions, collisional excitation and deexcitation, radiative and dielectronic recombination, and collisional inner-shell ionization and excitation. The $n = 3$ and above levels are treated as part of the continuum and interactions with an external radiation field are ignored. Transition probabilities and the appropriate ionization, recombination, and excitation rate coefficients have been taken from Refs. 26 and 27. In order to determine the density of heliumlike argon ions with one electron in an excited $n = 2$ level, the densities of heliumlike, hydrogenlike, and lithiumlike argon in their respective ground states must first be known. As an example, in Fig. 4(a) are shown the fractional abundances (proportional to the radial density profiles) of various charge states of argon (normalized to the flat total argon density) assuming that coronal equilibrium obtains. The same electron density and temperature profiles mentioned at the end of Sec. IV have been used in the calculations. The $^{18}\text{Ar}^{16+}$ profile is relatively flat out to 8 cm and then rapidly falls off. The $^{18}\text{Ar}^{17+}$ profile is centrally peaked while the $^{18}\text{Ar}^{15+}$ profile is hollow with a maximum in the shell structure near 8.5 cm.

The radial brightness profiles may now be calculated.

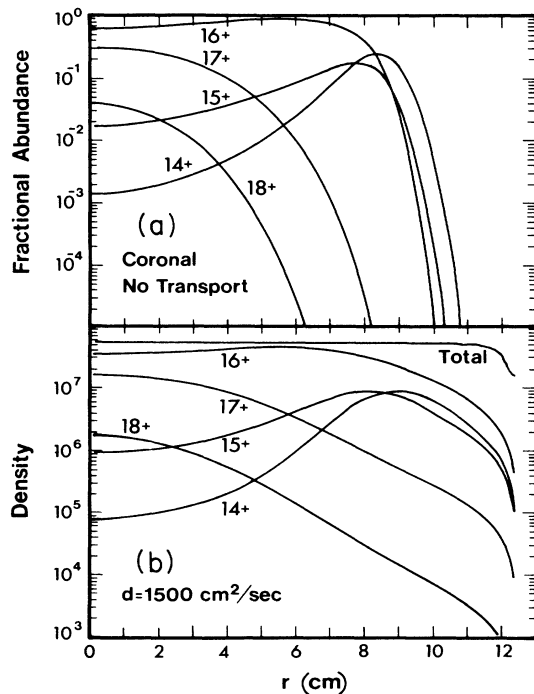


FIG. 4. Density profiles of the different charge states of argon (a) assuming coronal equilibrium and (b) including anomalous impurity transport.

As a starting point, it is assumed that electron-impact excitation from the ground state of $^{18}\text{Ar}^{16+}$ is the only population mechanism for the $n = 2$ levels. Again, measured electron density and temperature profiles as mentioned above are used, and the instrumental spatial resolution of 3 cm has been folded in. The calculated brightness profiles for the resonance, intercombination, and forbidden lines are shown in Fig. 5(a) for the charge-state profiles of Fig. 4(a). The profiles of the four lines are much narrower than the observed profiles of Fig. 3 and do not exhibit the crossing of the triplet profiles by the resonance line (singlet) profile. Inclusion of dielectronic and radiative recombination as upper-level population processes does not substantially improve matters, as shown in Fig. 5(b), mainly because of the lack of sufficient hydrogenlike argon at the outer radii [as shown in Fig. 4(a)], for the recombination to occur. There is, however, about a factor of 2 increase of the triplet lines relative to the resonance line.

From impurity transport studies performed on Alcator-C,²⁸ it is known that radial transport times can be shorter than certain recombination times. In fact, the diffusion coefficients used to describe the observed impurity transport are much greater than the theoretical neoclassical values. This would imply that impurity transport can cause charge state distributions to depart seriously from the coronal equilibrium values. This is demonstrated in Fig. 4(b), where the ionization-state density profiles calculated from an impurity transport code, using an anomalous impurity diffusion coefficient of $1500 \text{ cm}^2/\text{sec}$ (consistent with the results of Ref. 28), are shown for

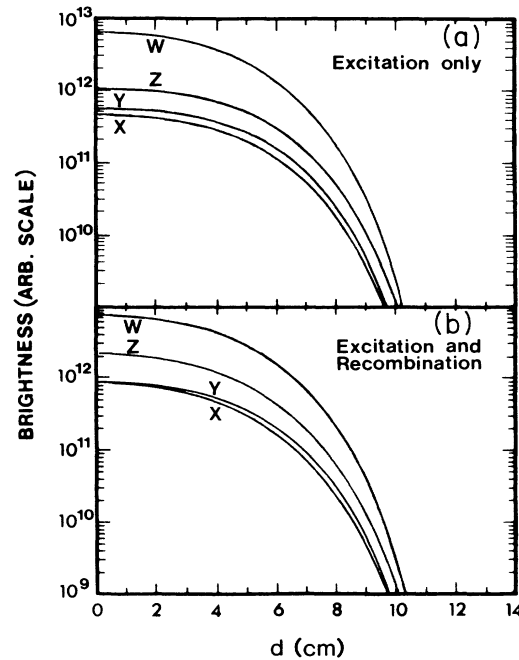


FIG. 5. Calculated brightness profiles for the coronal equilibrium density profiles (a) with collisional excitation as the only population mechanism and (b) including excitation and recombination.

comparison. The densities of heliumlike, lithiumlike, and berylliumlike argon are similar for the two cases inside a radius of 8 cm, but at 10 cm the heliumlike density for the case with transport is 4 orders of magnitude higher than the coronal equilibrium case. The hydrogenlike density profiles are similar inside 3 cm for the two figures, but in the transport case there is an enhancement of 10^3 at 8 cm. At 10 cm the difference is about 8 orders of magnitude. This indicates that impurity transport is an important consideration when interpreting brightness profiles, especially when recombination of ${}_{18}\text{Ar}^{17+}$ is significant.

Shown in Fig. 6(a) are the predicted brightness profiles when anomalous impurity transport is included in the calculation of the charge-state density profiles, and when the only population mechanism of the $n=2$ levels is collisional excitation. Again, these profiles do not agree with the observations. Shown in Fig. 6(b) are the brightness profiles for the resonance, intercombination, and forbidden lines when radiative and dielectronic recombination are included as population processes for excited $n=2$ levels in ${}_{18}\text{Ar}^{16+}$. While there is little change of the profiles inside of 6 cm, the brightnesses are greatly enhanced in the cooler regions of the plasma. The forbidden and intercombination line brightness profiles are predicted to be broader than the resonance line profile, in agreement with the observations. The conclusion is that in the outer regions of the plasma, recombination is the dominant population mechanism for the $n=2$ triplet states, and this is only possible because the impurity transport effects provide hydrogenlike argon in sufficient quantities.

While there is qualitative agreement between the model predictions and the observations, the relative intensities of

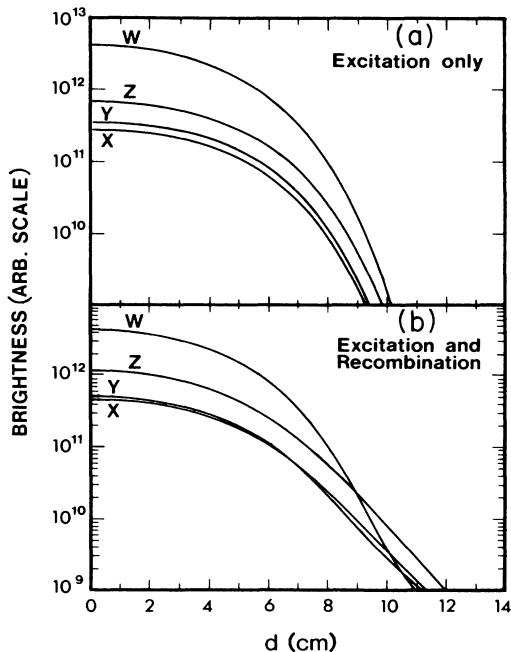


FIG. 6. Calculated brightness profiles for the anomalous impurity transport density profiles (a) for excitation only and (b) including recombination.

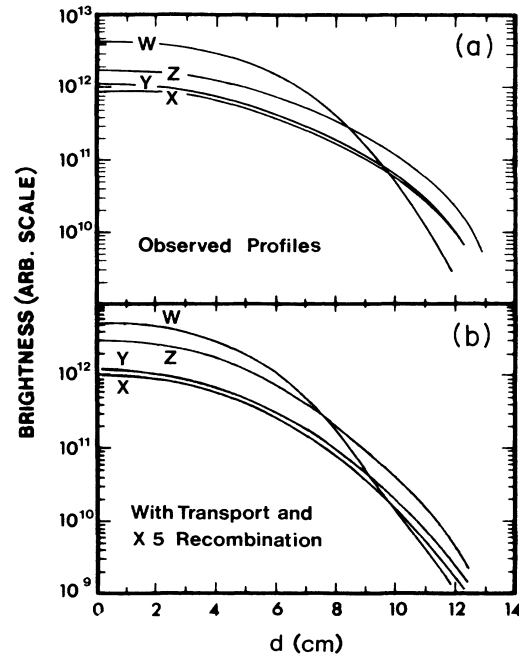


FIG. 7. (a) Observed brightness profiles and (b) calculated profiles including transport, excitation, and recombination enhanced by a factor of 5.

the resonance and forbidden lines are not exact, as the crossing point is observed to occur near 8 cm instead of at 9 cm as predicted. If the recombination rate coefficients are all increased by a factor of 5, the relative intensities are in quantitative accord, as shown in Fig. 7(b). In Fig. 7(a), the observed profiles of Fig. 3 are reproduced on the same scale for comparison. It is possible that the recombination rates of Ref. 26 are too small, although it is likely that the treatment of all levels with $n=3$ and above as part of the continuum is a possible source of the disagreement since cascades to different $n=2$ levels following recombination into higher- n levels have not been properly treated.²⁹ There are also uncertainties in the hydrogenlike argon density profiles calculated from the impurity transport code which could affect the size of the contribution from radiative recombination. These uncertainties arise from uncertainties in the possible spatial variation of the diffusion coefficient, and in the electron temperature profile. It has been suggested⁹ that charge-exchange recombination is a process that can be important for populating the $n=2$ triplet levels following cascades from higher n levels. In Sec. VI are presented direct observations of charge-exchange recombination which may have a bearing on the profiles of $\Delta n = 1$ transitions in ${}_{18}\text{Ar}^{16+}$.

VI. HIGH- n SPECTRA OF ${}_{18}\text{Ar}^{16+}$ AND CHARGE-EXCHANGE RECOMBINATION

Shown in Fig. 8 is a spectrum of the $1snp-1s^2$ series in ${}_{18}\text{Ar}^{16+}$ in the wavelength region from 3.0 to 3.4 Å for n between 3 and 13. Plasma parameters for the hydrogen, 80-kG discharges for which this spectrum was obtained were $I_p = 410$ kA, $\bar{n}_e = 2.2 \times 10^{14}$ cm⁻³, and $T_{e0} = 1500$

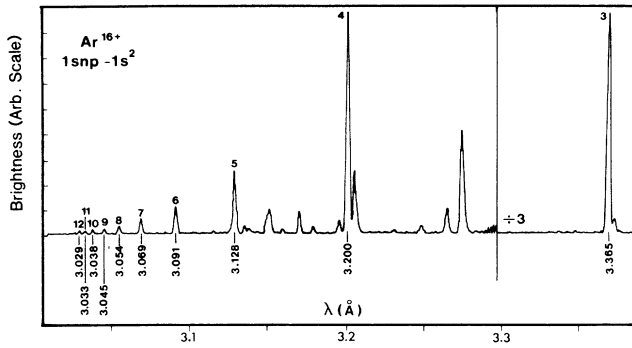


FIG. 8. Observations of $1snp-1s^2$ transitions in $^{18}\text{Ar}^{16+}$ for $3 < n < 12$ in the wavelength region from 3.0 to 3.4 Å.

eV. Wavelengths for the lines $1s5p-$ to $1s10p-1s^2$ have been taken from Ref. 30. Several satellites are apparent between 3.1 and 3.3 Å, and are discussed in Sec. IX. Wavelengths, relative intensities, and line identifications are given in Table II.^{31–33} The relative intensities of the $1snp-1s^2$ series for the central chord measurements are shown in Fig. 9 and are in agreement with the relative magnitude of the oscillator strengths³⁴ ($\propto n^{-3}$) which indicates that electron-impact excitation is the predominant mechanism for populating the upper levels. Shown in Fig. 10 are spectra from $1s7p-$ to $1s11p-1s^2$ transitions obtained at three different radial locations for a series of 80 kG, hydrogen discharges with a limiter radius of 16.5 cm. For the outer radii, the $1s9p-1s^2$ and $1s10p-1s^2$ lines are strongly enhanced relative to $1s7p-1s^2$, compared to the central spectrum.¹⁸ This suggests that there is a population mechanism which selects these particular levels. Charge transfer between neutral hydrogen and hydrogen-like argon should selectively populate levels around $n=9$ and $n=10$, since $^{18}\text{Ar}^{17+}$ is similar to fully stripped chlorine.³⁵ This process will be important in the cooler

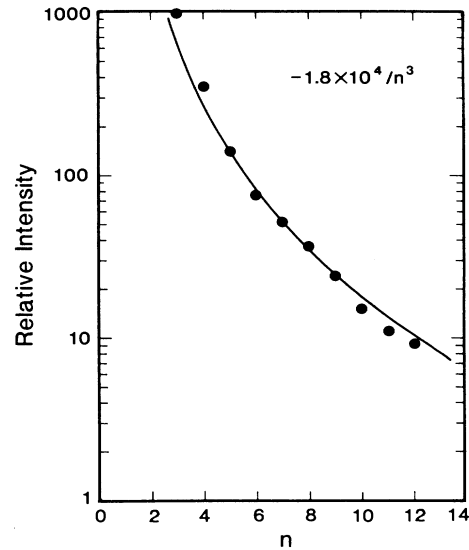


FIG. 9. The intensities of the central chord $1snp-1s^2$ lines as a function of n , compared to the oscillator strengths.

regions of the plasma where there is a large relative neutral density. By measuring the enhancement of the $1s9p-1s^2$ and $1s10p-1s^2$ transitions over the values expected from population by excitation and radiative recombination, the intrinsic neutral density and density profile can be determined, provided that the charge-transfer cross sections are known. Enhanced population of high- n levels in oxygen by charge-exchange recombination with intrinsic n_0 has been observed previously in ORMAK (Oak Ridge Tokamak).³⁶

The situation is different in helium working gas. In contrast to the hydrogen case, spectra obtained in ^4He do not exhibit a strong enhancement of the $1s9p-$ and $1s10p-1s^2$ transitions at the outer radii, as shown in Fig.

TABLE II. Wavelengths, relative intensities, and line identifications for $\Delta n > 1$ transitions.

Name	Transition	Rel. int.	λ	λ_S^{32}	$\lambda_{\text{BSFC}}^{31}$
$^{18}\text{Ar}^{16+}$	$1s3p-1s^2$		3.3654		
sat	$1s2p4p-1s^22p$	0.145	3.2728	3.2722	
sat	$1s2p4p-1s^22p$	0.310	3.2713	3.2709	3.270
sat	$1s2s4p-1s^22s$	0.083	3.2622	3.2629	3.259
sat		0.011	3.2469		
sat	$1s2s4p-1s^22p$	0.032	3.2454	3.2458	3.245
sat	$1s2p5p-1s^22p$	0.182	3.2046	3.2049	3.202
$^{18}\text{Ar}^{16+}$	$1s4p-1s^2$	1.000	3.1999		
sat	$1s2s5p-1s^22p$	0.050	3.1947	3.1949	3.192
sat		0.020	3.1784		
sat	$1s2p6p-1s^22p$	0.077	3.1693	3.1696	3.167
sat	$1s2s6p-1s^22s$	0.034	3.1590	3.1594	3.156
$^{18}\text{Ar}^{17+}$	$3p-1s$	0.096	3.1510		
sat	$1s2p7p-1s^22p$	0.065	3.1491		3.146
sat		0.008	3.1429	3.1433	
Mo?		0.027	3.1382		
sat		0.038	3.1349		
$^{18}\text{Ar}^{16+}$	$1s5p-1s^2$	0.449	3.1285		

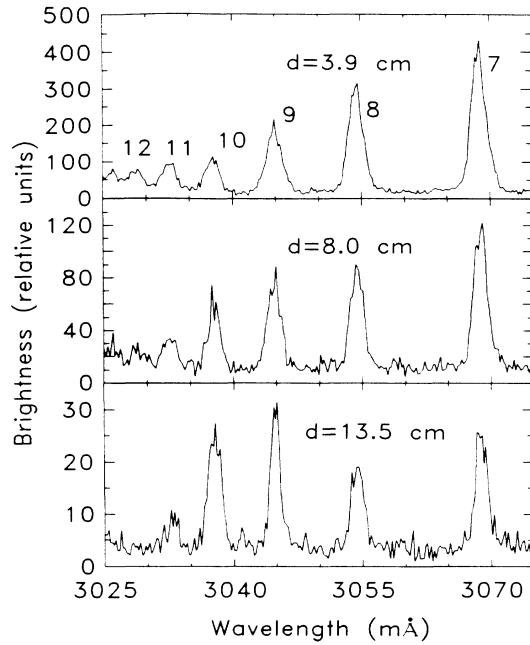


FIG. 10. Spectra from $1s7p-$ to $1s11p-1s^2$ transitions from three radial locations.

11. This is because there is no resonant transfer between neutral helium and ${}_{18}\text{Ar}^{17+}$ into levels near $n=9$.

Brightness profiles for the transitions $1s3p-1s^2$ to $1s12p-1s^2$, obtained during a series of 80 kG, hydrogen discharges with $\bar{n}_e = 1.8 \times 10^{14} \text{ cm}^{-3}$ and $T_{e0} = 1800 \text{ eV}$ are shown in Fig. 12. The limiter radius was 16.5 cm. All of the profiles are centrally peaked and rapidly fall off in intensity out to a chord of 8 cm. Outside of 8 cm, all the profiles tend to flatten out. The $1s9p-$ and $1s10p-1s^2$ profiles cross the $1s8p-1s^2$ curve at about 8 cm, while all the other profiles have a similar shape. A model similar to the one described in Sec. IV has been used to calculate the emissivity (and brightness) profiles of the $1snp-1s^2$ series for $3 < n < 13$. The line intensities are determined from a balance among radiative decay directly to the ground state, collisional excitation out of the ground state of heliumlike argon, and radiative and charge-exchange recombination of hydrogenlike argon in the ground state. In general, the emissivity of a $1snp-1s^2$ transition in ${}_{18}\text{Ar}^{16+}$ is given by

$$E_n(r) = n_e(r) [n_{\text{Ar}^{16+}}(r) \langle \sigma v \rangle_{n,\text{exc}}(r) + n_{\text{Ar}^{17+}}(r) \langle \sigma v \rangle_{n,\text{rr}}(r) + n_0(r) n_{\text{Ar}^{17+}}(r) \langle \sigma v \rangle_{n,\text{cx}}(r)], \quad (1)$$

where $n_0(r)$ is the neutral-hydrogen density and the subscripts exc, rr, and cx denote excitation, radiative recombination, and charge-transfer recombination. Radiative transitions to any levels except the ground state, collisional deexcitation and excitation from any other levels, ionization, cascades from upper levels, and dielectronic recombination have all been ignored. Excitation and radiative recombination rates have been taken from Ref. 27, and charge-exchange cross sections for fully stripped

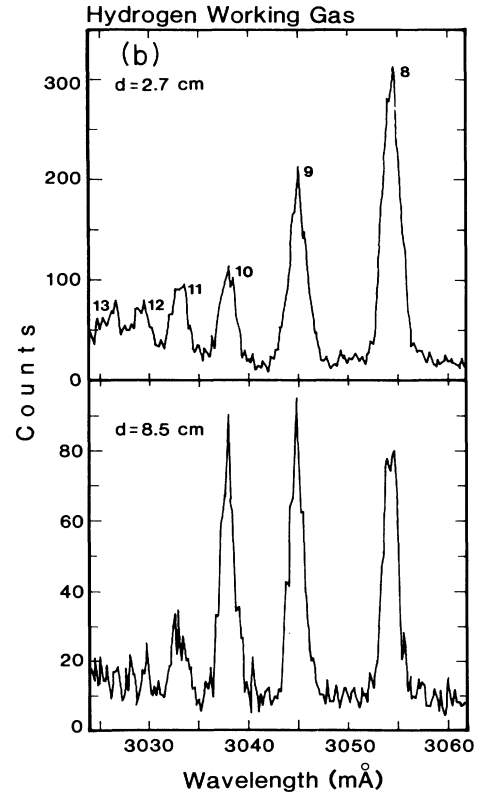
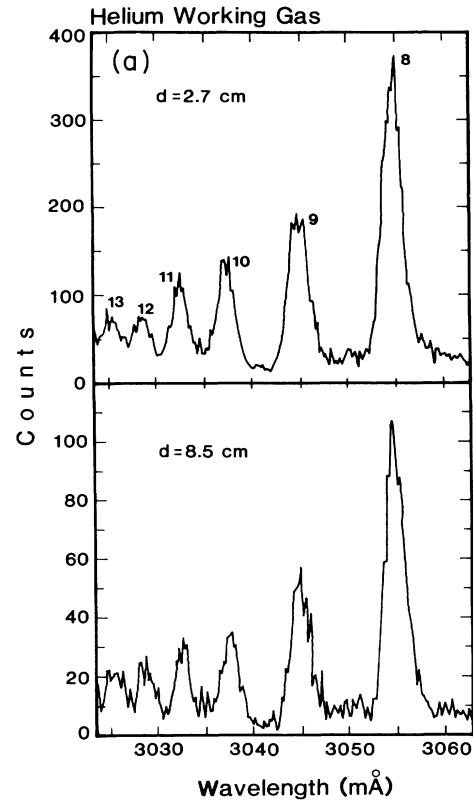


FIG. 11. Spectra from $1s8p-$ to $1s13p-1s^2$ transitions from two different chords obtained in (a) helium working gas and (b) hydrogen working gas.

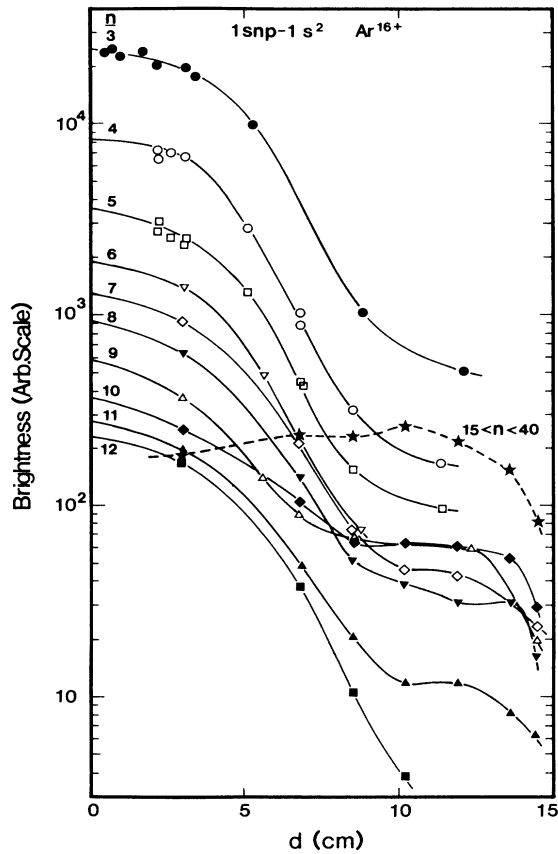


FIG. 12. Observed brightness profiles of $1snp-1s^2$ transitions in $^{18}\text{Ar}^{16+}$.

chlorine (to model hydrogenlike argon) have been interpolated from Ref. 35. Density profiles for hydrogenlike and heliumlike argon have again been determined from the code modeling, including the effects of anomalous impurity transport. Shown in Fig. 13 are the calculated emissivity profiles for $1s3p$ - to $1s12p-1s^2$ transitions, demonstrating the individual effects of excitation (a), radiative recombination (b), and charge-exchange recombination (c), in addition to the composite profiles of excitation and radiative recombination (d) and the grand total (e). Plasma parameters for these calculations were $T_{e0}=1800$ eV, $a_T=10$ cm, $n_{e0}=2.2 \times 10^{14}$ cm $^{-3}$, $a_L=16.5$ cm, $\alpha=0.5$, $T_i=0.8 T_e$, and

$$n_0 = (5 \times 10^6 \text{ cm}^{-3}) \{1 + 0.00347 \exp[0.815r(\text{cm})]\}.$$

It is apparent that collisional excitation is most important inside of 10 cm while radiative recombination dominates between 10 cm and the limiter radius for most of the lines. Charge-transfer recombination is only important for the $n=8, 9$, and 10 levels at the outer radii although it may contribute to lower n levels following subsequent cascades. It has been assumed that 25% of the charge transfer occurs into the p levels,³⁷ l mixing³⁸ has been ignored and it has been assumed that $\frac{1}{4}$ of the charge transfer occurs into singlet levels, the states which pri-

marily give rise to observed x rays. These factors have been included in $\langle \sigma v \rangle_{n,cx}$ in Eq. 1.

Brightness profiles for these conditions, obtained from the calculated emissivity profiles, assuming an instrumental spatial resolution of 3 cm, are shown in Fig. 14. These calculated brightness profiles are in good agreement with observations, demonstrated in Fig. 12. Emissivity profiles obtained from Abel inversion of the observed brightness profiles, along with calculated profiles, can be found in Ref. 18. In Fig. 15 are shown the radial profiles of the ratios of brightnesses of $1snp-1s^2$ transitions to the $1s7p-1s^2$ line for $n=8, 9, 10$, and 11. The enhancement for $n=9$ and $n=10$ becomes very apparent beyond 8 cm. This enhancement, which is attributed entirely to charge-exchange recombination, may be used to calculate the neutral-density profile.

With regard to the issue of whether or not charge-exchange recombination is responsible for the broad triplet line profiles, it is not possible to make a definite conclusion at this time. The evidence suggests that a recombination process is responsible, as in Fig. 7, and there is certainly evidence that charge-exchange recombination is occurring under certain operating conditions, as shown in this section. But until detailed cascade calculations from high- n levels around 9 and 10 to the $n=2$ level are performed, it is difficult to claim that charge-exchange recombination is the source of the broad triplet $n=2$ profiles. Observations of the triplet line profiles have been made in helium working gas, and are similar to those in hydrogen. These profiles might be expected to be different if charge exchange, which is certainly different in helium plasmas, is important. However, for similar operating conditions as in hydrogen, helium plasmas have different electron temperature profiles and the impurity transport is quite different so a direct comparison is not possible.

VII. NEUTRAL-DENSITY PROFILES

Since the spectrometer system does not have an absolute intensity calibration and since the absolute argon density in the plasma is not directly measured, the product of these two factors can be determined by comparison of the observed emissivity of a particular line, $e_n(r)$, and the calculated emissivity from Eq. (1), $E_n(r)$. For the central emissivity of the $1s7p-1s^2$ line, for example, charge-exchange recombination is negligible, and the relative emissivity is

$$e_7(0) = A n_e(0) \langle \sigma v \rangle_{7,exc}(0) + n_{\text{Ar}^{17+}}(0) / n_{\text{Ar}^{16+}}(0) \langle \sigma v \rangle_{7,rr}(0), \quad (2)$$

where A is the normalization constant which includes the effects of detector sensitivity, crystal reflectivity, viewed solid angle, window transmission, and total argon density. The cross sections are known functions of electron temperature, the electron density is measured, the ratio of hydrogenlike to heliumlike argon densities is determined

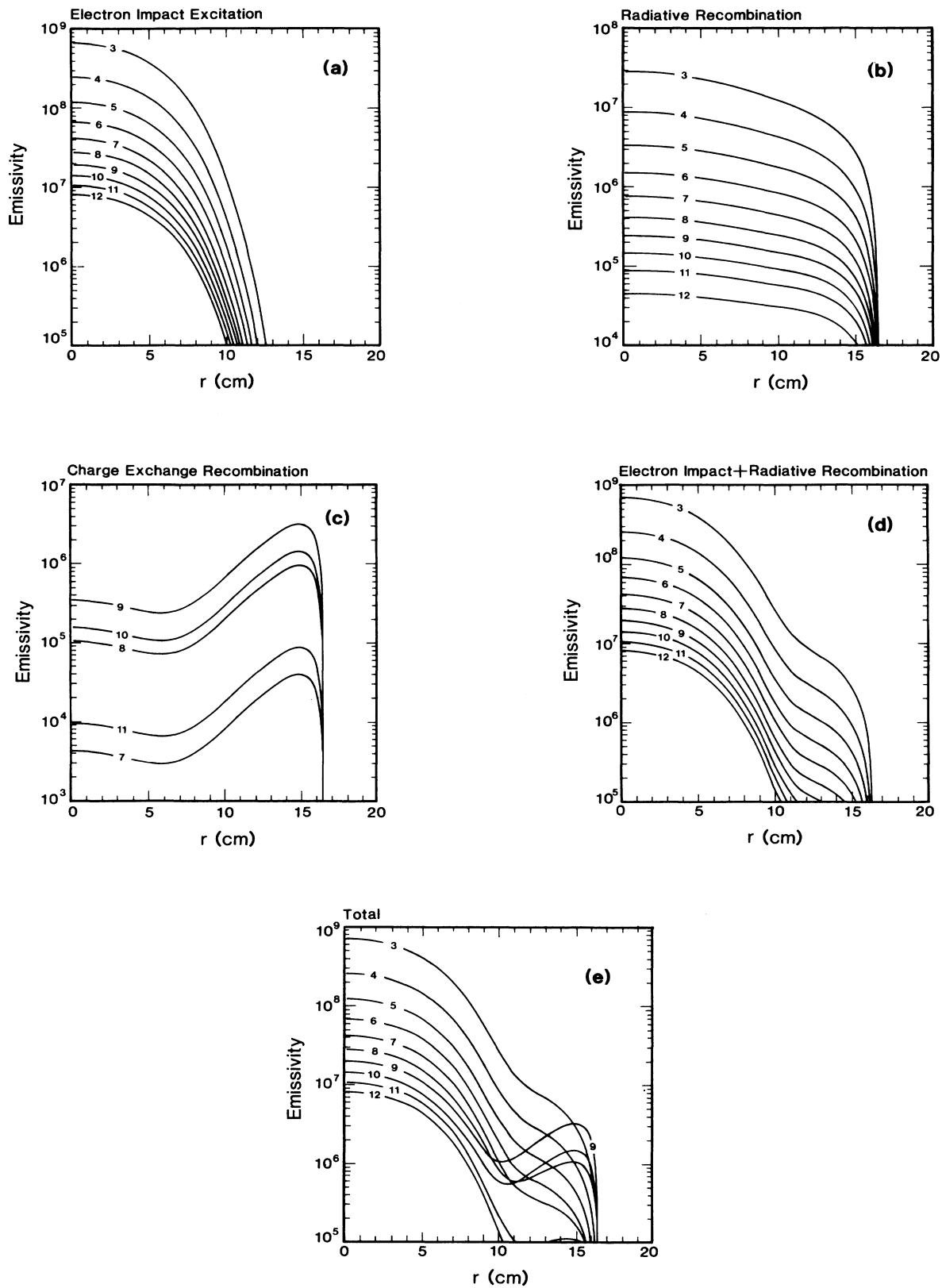


FIG. 13. Calculated emissivity profiles for $1snp-1s^2$ transitions of $^{18}\text{Ar}^{16+}$ assuming the upper levels were populated by (a) collisional excitation, (b) radiative recombination, (c) charge-exchange recombination, (d) collisional excitation and radiative recombination, and (e) the grand composite of (a), (b), and (c).

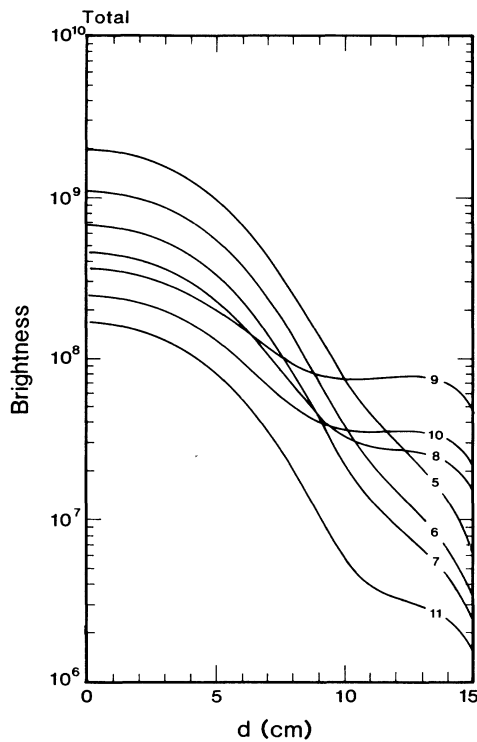
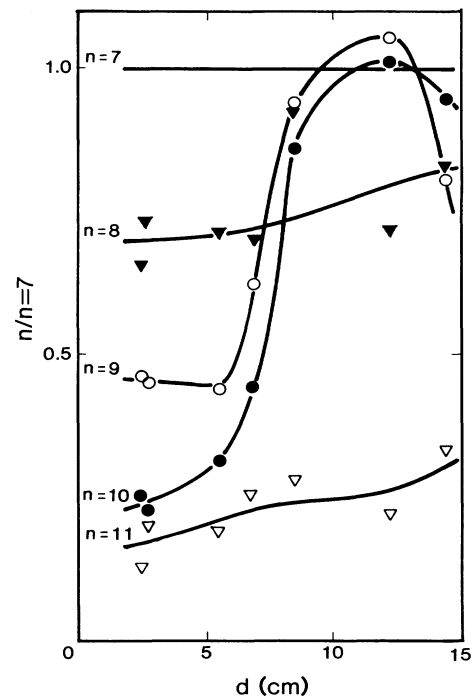


FIG. 14. Calculated brightness profiles from Fig. 13(e).

from the transport code, and the central relative emissivity is obtained from Abel inversion of the observed brightness profile of the $1s\ 7p-1s^2$ line. This determines the normalization constant A . The neutral-hydrogen density

$$n_0(r) = \frac{e_9(r)/A - n_e(r)[\langle\sigma v\rangle_{9,\text{exc}}(r) + n_{\text{Ar}^{17+}}(r)/n_{\text{Ar}^{16+}}(r)\langle\sigma v\rangle_{9,\text{rr}}(r)]}{\langle\sigma v\rangle_{9,\text{cx}}(r)n_{\text{Ar}^{17+}}(r)/n_{\text{Ar}^{16+}}(r)} \quad (3)$$

An example of a neutral-density profile determined in this fashion from the $1s\ 9p-1s^2$ and $1s\ 10p-1s^2$ emissivities is shown in Fig. 16. The inferred neutral density increases 2 orders of magnitude in going from $2 \times 10^7\ \text{cm}^{-3}$ at 9 cm to $2 \times 10^9\ \text{cm}^{-3}$ at 14 cm. Also plotted are neutral-density profiles calculated from the FRANTIC neutral transport code.³⁹ The agreement is quite good although there are several uncertainties in both the calculations and measurements. These measurements were obtained at a limiter port, which may have a different neutral density than at other toroidal locations.⁴⁰ There are also known to be poloidal asymmetries in edge conditions⁴¹ which can affect conclusions about the neutral-density profile. Another source of uncertainty in these neutral-density profile estimates is that values of the $_{18}\text{Ar}^{17+}$ to $_{18}\text{Ar}^{16+}$ ratios were obtained from the results of the impurity transport code simulations.

FIG. 15. Radial profiles of the intensity ratios of $1snp-$ to $1s\ 7p-1s^2$ with $n = 8, 9, 10,$ and 11 .

profile can then be determined from Eq. 1 using a transition for which charge-exchange recombination is important. For the $1s\ 9p-1s^2$ line, for example, the neutral density may be found from

VIII. VERY-HIGH- n TRANSITIONS IN $_{18}\text{Ar}^{16+}$

The concern of Sec. VI was the effect of charge-transfer recombination between $_{18}\text{Ar}^{17+}$ and neutral hydrogen in the ground state. As was shown, there is a large enhancement at the plasma edge of the $1s\ 9p-$ and $1s\ 10p-1s^2$ transitions in $_{18}\text{Ar}^{16+}$. At slightly shorter wavelengths there is an even larger manifestation¹⁸ of charge-exchange recombination, as shown in Fig. 17. This is a spectrum in the vicinity of the ionization limit of $_{18}\text{Ar}^{16+}$ obtained from the plasma periphery for a series of 80-kG, hydrogen discharges with $\bar{n}_e = 1.8 \times 10^{14}\ \text{cm}^{-3}$ and $T_{e0} = 1800$ eV. There is a broad emission feature between 3009 and 3020 mÅ which has a maximum at 3013 mÅ and a shoulder at 3017 mÅ. The series limit is at 3008.8 mÅ. The peak and the shoulder occur near the wavelengths for the $1s\ 27p-1s^2$ and $1s\ 18p-1s^2$ transitions, respectively, in

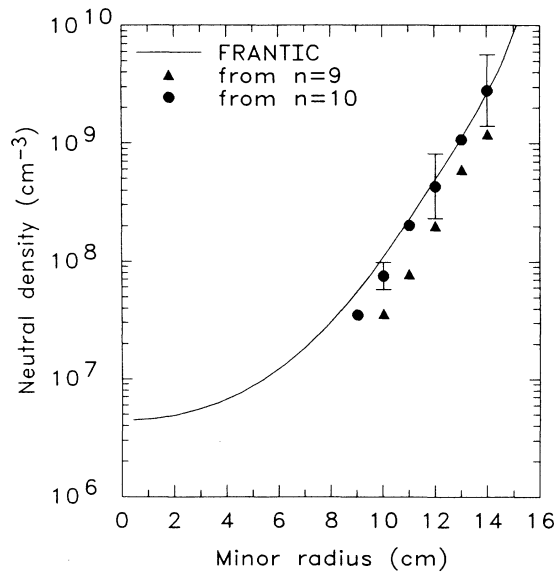


FIG. 16. Neutral hydrogen density profiles obtained from the charge-transfer enhancements of the $1s9p-1s^2$ and $1s10p-1s^2$ transitions over the calculated values from population by excitation and radiative recombination. FRANTIC code calculations are shown for comparison.

$^{18}\text{Ar}^{16+}$. These are integral multiples of $n=9$, the level into which charge transfer occurs from neutral hydrogen in the ground state. The upper levels of these lines are populated by charge transfer from neutral hydrogen in the excited $n=3$ and $n=2$ levels,⁴² respectively. The radial brightness profile of this feature is included in Fig. 12 and

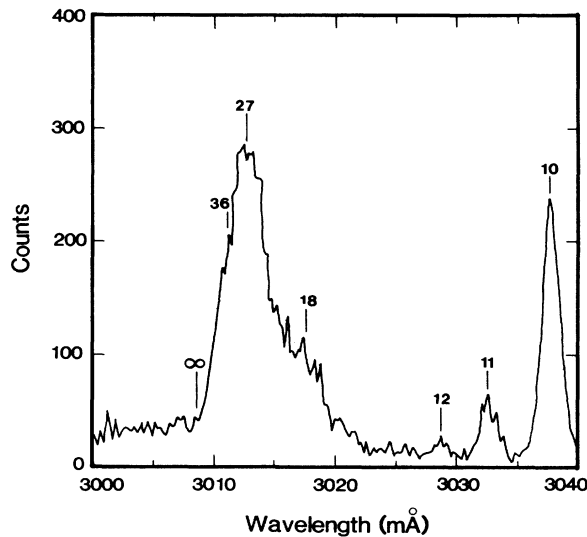


FIG. 17. Spectrum from transitions of very-high- n levels to the ground state in the vicinity of the ionization limit of $^{18}\text{Ar}^{16+}$.

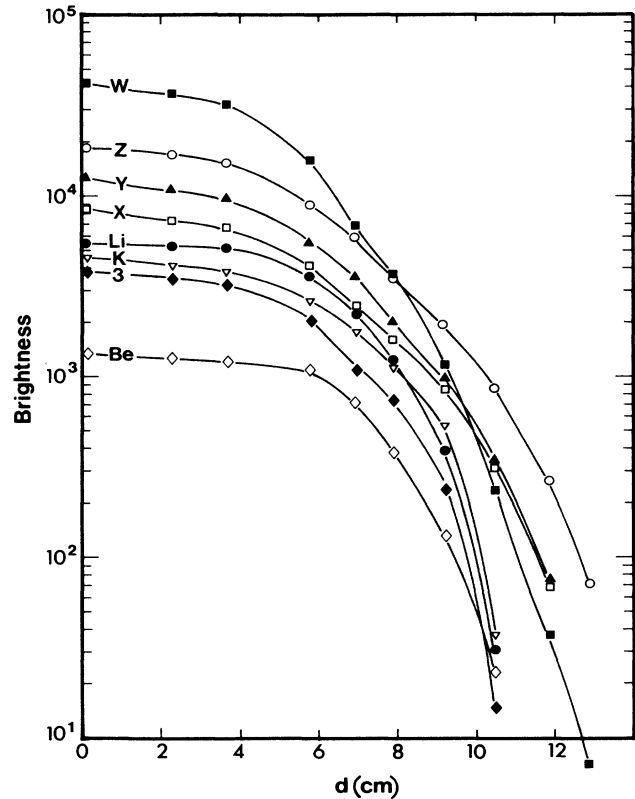


FIG. 18. Radial profiles of satellites to $n=2$ to $n=1$ transitions.

the maximum emission emanates from the plasma edge, near $r=13$ cm, indicating that this feature is populated by a recombination process.

IX. SATELLITE LINES AND RADIAL PROFILES

In Secs. IV and VI were presented radial brightness profiles of ground-state transitions in heliumlike argon. Close in wavelength to these transitions are satellites due to lithiumlike and berylliumlike argon. Radial profiles of the satellites tend to be broader than the corresponding heliumlike profiles because at least some of the upper levels are formed by dielectronic recombination which has a weaker temperature dependence than collisional excitation. Radial brightness profiles of the satellites to the $n=2$ upper-level spectra are shown in Fig. 18. Li indicates the sum of all lines between 3.975 and 3.987 Å (q, r, and a), 3 corresponds to the $n=3$ spectator transitions between 3.953 and 3.957 Å, and Be is due to all lines between 4.007 and 4.023 Å. The satellite profiles are all relatively flat near the plasma center and then fall off extremely rapidly outside of 9 cm.

The satellites to the $n > 3$ ground-state transitions exhibit similar behavior. Shown in Fig. 19 are spectra in the wavelength region from 3.13 to 3.22 Å from three discharges with $a_L = 16.5$ cm. Wavelengths and line identifications are given in Table II and will be discussed in detail in a forthcoming paper.³³ About halfway out in

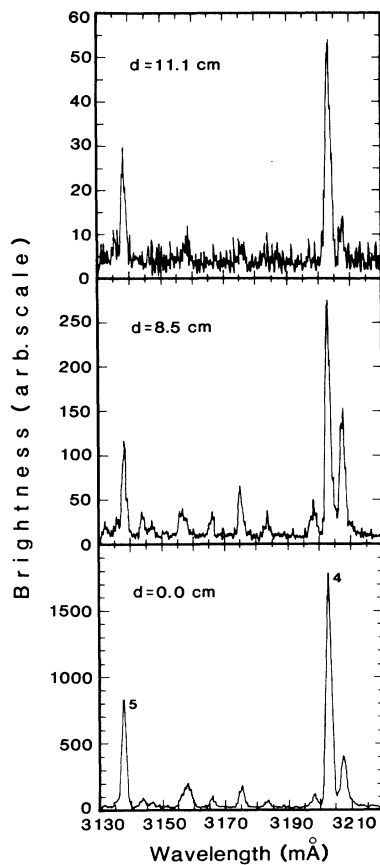


FIG. 19. Spectra of satellites in the vicinity of the $1s4p$ - and $1s5p$ - $1s^2$ lines for three radial locations.

minor radius (8.5 cm) the satellites have grown significantly with respect to the $1s4p$ - and $1s5p$ - $1s^2$ transitions. (The satellites in this region are mainly due to $n=2$ spectator electrons perturbing the $1s5p$ - and $1s6p$ - $1s^2$ transitions.) The satellites all abruptly disappear at a slightly larger minor radius. Shown in Fig. 20 are radial profiles of the brightness ratios of the satellite lines to the $1s4p$ - $1s^2$ transition. These curves have a strong maximum at 8.5 cm, which depends on the particular temperature profile shape for given operating conditions.

X. CONCLUSIONS

Spectra and radial brightness profiles of all the ground-state transitions in heliumlike argon have been obtained. Modeling of the line intensities of $\Delta n=1$ ground-state transitions indicates that for the plasma center, electron-impact excitation is the strongest population process for the upper levels. In the cooler outer regions of the plasma, radiative recombination of hydrogenlike argon is very important for populating the upper levels in $^{18}\text{Ar}^{16+}$. Fast impurity transport from the plasma center is crucial in providing sufficient $^{18}\text{Ar}^{17+}$ in the cooler regions for the recombination to occur. Near the limiter radius, there is an excess of emission in the triplet

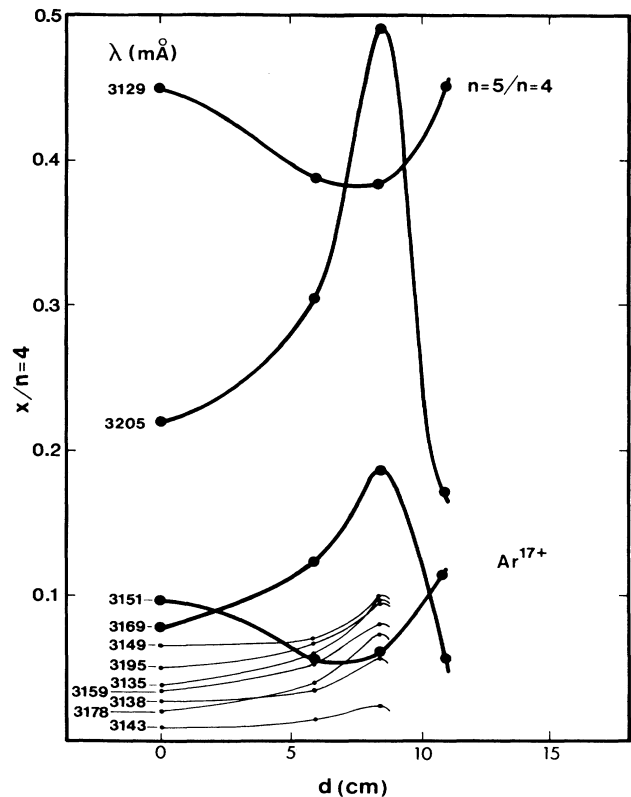


FIG. 20. Radial profiles of the brightness ratios of satellites and the $1s4p$ - $1s^2$ transition.

lines over that expected from the line intensity model. This is possibly due to the improper treatment of cascades from upper levels in heliumlike argon, which themselves have been populated by radiative and perhaps charge-transfer recombination. There are, however, several uncertainties in the calculated edge line intensities due to uncertainties in the edge electron temperature and hydrogenlike argon abundance. Radial profiles of $\Delta n > 1$ ground-state transitions have also been measured, and similar to the $\Delta n=1$ transitions, excitation is most important in populating the upper levels near the plasma center, while radiative recombination dominates at the edge. For the transitions $1s9p$ - and $1s10p$ - $1s^2$, charge-exchange recombination from intrinsic neutral hydrogen is by far the most important population process near the plasma edge. The intensities of these lines have been used to deduce neutral hydrogen density profiles. High- n transitions ($1snp$ - $1s^2$, with $13 < n < 40$) have been observed to be populated solely by charge transfer between excited neutral hydrogen and $^{18}\text{Ar}^{17+}$.

ACKNOWLEDGMENTS

Operation of the Alcator-C tokamak by D. Gwinn and B. Lipschultz is gratefully acknowledged. Calculations by C. Fiore and V. Safronova, data reduction by M. Ono, and support from R. Parker are also appreciated. This work was supported by U.S. Department of Energy Contract No. DE-AC02-78ET51013.

- ¹M. Bitter *et al.*, Phys. Rev. Lett. **42**, 304 (1979).
²M. Bitter *et al.*, Phys. Rev. Lett. **43**, 129 (1979).
³M. Bitter *et al.*, Phys. Rev. Lett. **47**, 921 (1981).
⁴E. Källne *et al.*, Phys. Rev. Lett. **49**, 330 (1982).
⁵F. Bely-Dubau *et al.*, Phys. Rev. A **26**, 3459 (1982).
⁶E. Källne *et al.*, Phys. Rev. A **27**, 2682 (1983).
⁷M. L. Apicella *et al.*, Phys. Rev. Lett. **98A**, 174 (1983).
⁸E. Källne *et al.*, Phys. Rev. A **28**, 467 (1983).
⁹E. Källne *et al.*, Phys. Rev. Lett. **52**, 2245 (1984).
¹⁰M. Bitter *et al.*, Phys. Rev. A **29**, 661 (1984).
¹¹P. Lee *et al.*, Phys. Rev. A **31**, 3996 (1985).
¹²P. Lee *et al.*, Phys. Rev. Lett. **55**, 386 (1985).
¹³R. Bartiromo *et al.*, Phys. Rev. A **32**, 531 (1985).
¹⁴TFR Group *et al.*, Phys. Rev. A **32**, 2374 (1985); **32**, 3000 (1985).
¹⁵M. Bitter *et al.*, Phys. Rev. A **32**, 3011 (1985).
¹⁶E. Källne *et al.*, Nucl. Instrum. Methods Phys. Res. B **9**, 698 (1985).
¹⁷E. Källne *et al.*, Phys. Scr. **31**, 551 (1985).
¹⁸J. E. Rice *et al.*, Phys. Rev. Lett. **56**, 50 (1986).
¹⁹E. S. Marmar *et al.*, Phys. Rev. A **33**, 774 (1986).
²⁰P. Lee *et al.*, Phys. Rev. A **34**, 3210 (1986).
²¹B. Blackwell *et al.*, in *Plasma Physics and Controlled Nuclear Fusion Research, 1982* (International Atomic Energy Agency, Vienna, 1983), Vol. II, p. 27.
²²J. Källne *et al.*, Nucl. Instrum. Methods **203**, 415 (1982).
²³L. A. Vainshtein and U. I. Safronova, At. Data Nucl. Data Tables **21**, 49 (1978); **25**, 311 (1980).
²⁴C. P. Bhalla and T. W. Tunnel, J. Quant. Spectrosc. Radiat. Transfer **32**, 141 (1984).
²⁵L. A. Vainshtein and V. I. Safronova, Phys. Scr. **31**, 519 (1985).
²⁶R. Mewe and J. Schrijver, Astron. Astrophys. **65**, 99 (1978).
²⁷R. C. Isler, Nucl. Fusion **24**, 1599 (1984).
²⁸E. S. Marmar *et al.*, Nucl. Fusion **22**, 1567 (1982).
²⁹A. Pradhan, Astrophys. J. **288**, 824 (1985).
³⁰J. F. Seely and U. Feldman, Phys. Rev. Lett. **54**, 1016 (1985).
³¹P. G. Burkhalter *et al.*, J. Appl. Phys. **50**, 532 (1979).
³²U. I. Safronova (private communication).
³³E. Källne *et al.* (unpublished).
³⁴W. L. Wiese, M. W. Smith, and B. M. Glennon, *Atomic Transition Probabilities*, Natl. Bur. Stand. (U.S.), Natl. Stand. Ref. Data Ser. No. 4 (U.S. GPO, Washington, D.C., 1966).
³⁵R. K. Janev, D. S. Belic, and B. H. Bransden, Phys. Rev. A **28**, 1293 (1983).
³⁶R. C. Isler and E. C. Crume, Phys. Rev. Lett. **41**, 1296 (1978).
³⁷V. A. Abramov, F. F. Baryshnikov, and V. S. Lisitsa, Pis'ma Zh. Eksp. Teor. Fiz. **27**, 494 (1978) [JETP Lett. **27**, 465 (1978)].
³⁸R. Fonck *et al.*, Phys. Rev. A **29**, 3288 (1984).
³⁹C. L. Fiore (private communication).
⁴⁰E. S. Marmar, J. Nucl. Mater. **76&77**, 59 (1978).
⁴¹B. Lipschultz *et al.*, Nucl. Fusion **24**, 977 (1985).
⁴²R. Olson, J. Phys. B **13**, 483 (1980).